ACADÉMIE
DES SCIENCES
INSTITUT DE FRANCE

Comptes Rendus
Mécanique

Rawad Wakim, Quentin Javey, Christian Gentil, Cristian Ovalle Rodas, Lucien Laiarinandrasana and Alain Thionnet

A homogenization technique for materials with periodic lacunar fractal microstructure

Volume 353 (2025), p. 1185-1200

Online since: 21 November 2025

https://doi.org/10.5802/crmeca.330

The Comptes Rendus. Mécanique *are a member of the Mersenne Center for open scientific publishing*
www.centre-mersenne.org — e-ISSN : 1873-7234

ACADÉMIE DES SCIENCES
INSTITUT DE FRANCE

Comptes Rendus. Mécanique
2025, Vol. 353, p. 1185-1200
https://doi.org/10.5802/crmeca.330

Research article

A homogenization technique for materials with periodic lacunar fractal microstructure

Rawad Wakim [*,a], **Quentin Javey** [a], **Christian Gentil** [b], **Cristian Ovalle Rodas** [a], **Lucien Laiarinandrasana** [a] **and Alain Thionnet** [a,c]

[a] Mines Paris, PSL University, Centre for Material Sciences (MAT), CNRS UMR 7633, 78000 Versailles, France

[b] LIB UR 7534, Université Bourgogne Europe, 21000 Dijon, France

[c] Université Bourgogne Europe, 21000 Dijon, France

E-mails: rawad.wakim@minesparis.psl.eu, quentin.javey@minesparis.psl.eu, christian.gentil@ube.fr, cristian.ovalle_rodas@minesparis.psl.eu, lucien.laiarinandrasana@minesparis.psl.eu, alain.thionnet@minesparis.psl.eu, alain.thionnet@ube.fr

Abstract. This paper proposes an original homogenization approach for materials characterized by a periodic lacunar microstructure with fractal geometry. The geometrical complexity of these materials creates major difficulties for the application of conventional homogenization methods to evaluate their effective properties. As the fractal level increases, the number of degrees of freedom in the numerical models grows sharply, making the computations very expensive and, beyond a certain level, inaccessible. To address this challenge, an indirect homogenization technique was developed on the basis of a classical direct homogenization technique (periodic homogenization by the average method), by embedding into this homogenization process the iterative process of generating fractal geometries following the iterated function systems principle. The two techniques were applied to two-dimensional extruded geometries and to a fully three-dimensional case. For iteration levels where both techniques could be compared, their results were very close. In addition, the indirect technique is substantially more efficient, requiring lower computational cost in terms of time and memory, and enabling the study of iteration levels that cannot be reached with the direct one. Finally, when the iteration level tends to infinity the theoretical and numerical convergence values of the homogenized elasticity tensors are equal. This provides direct proof of the quality of the method.

Keywords. Homogenization, fractal geometries, lacunar materials.

Funding. This work is part of the ITERATE project (ANR-20-CE46-0011), which involves four partners: ALTAIR, CT-IPC (Industrial Technical Center for Plastics and Composites), LIB (Laboratoire d'Informatique de Bourgogne), and CdM (Centre for Material Sciences). The authors would like to thank all project partners for their collaboration, and the ANR (French National Research Agency) for its support of this project.

Manuscript received 27 August 2025, revised 7 October 2025, accepted 10 October 2025.

* Corresponding author

1. Introduction

Fractal geometry, synthesized and popularized by Mandelbrot in 1975 [1], is characterized by self-similarity across scales. Only elementary aspects of this concept are required here. A self-similar pattern is said to be of level-n when similarity is observed over n successive lower scales. Fractal concepts have been used in diverse fields, including mass and heat transfer [2], architecture [3], antennas [4,5], jewelry [6], and pharmaceuticals [7].

Regarding the mechanical properties of materials with a fractal lacunar microstructure, the literature appears limited. Studies that are closest in spirit mostly investigate the structural response of fractal structures [8–14]. The present study addresses this gap by investigating the effective mechanical properties of materials with a fractal lacunar microstructure.

Homogenization is the most widely recognized approach for calculating the equivalent properties of a material with a heterogeneous microstructure. Its fundamental principles have been firmly established for many years [15–21]. However, solving the equations induced by this technique generally requires a numerical procedure, particularly the finite element method, since analytical solutions are unlikely to exist in most cases of practical interest.

When applied to fractal lacunar geometries, this numerical approach faces a specific challenge: the number of Degrees Of Freedom (DOFs) in the discretized problem grows rapidly with the fractal iteration level. This sharp increase in problem size makes the computations very costly in terms of time and computational resources. For illustration, consider the case of a Menger sponge (Figure 3): a level-4 sponge contains 160 000 level-0 units. If each level-0 unit is discretized with 100 hexahedral elements, the total reaches 16×10^6 elements, highlighting the rapid increase in problem size as the iteration level rises.

Accordingly, the objective of this paper is to develop an Adapted Homogenization Technique (AHT), based on a Usual Homogenization Technique (UHT), suitable for predicting the equivalent elastic behavior, particularly the fourth-order elasticity tensor, denoted $\underset{\approx}{C}{}_n^H$, of a level-$n$ Fractal Microstructure Material (FMMn), while reducing computation time and the need for computational resources.

2. Choice of UHT used to build the AHT: periodic homogenization technique by the average method

Among several established homogenization strategies based on the so-called averaging technique, two classical approaches are commonly distinguished: the Effective Moduli Homogenization Technique (EMHT) and the Periodic Homogenization Technique by the Average Method (PHT). Their main characteristics are:

- EMHT:
  - applicable to materials whose microstructure is not necessarily periodic;
  - primal (stress-based) and dual (strain-based) formulations are not equivalent;
  - for periodic materials, the result depends on the geometric period selected.
- PHT:
  - applicable to materials with a periodic microstructure;
  - for linear elastic constituents, several theorems and properties guarantee existence and uniqueness of solutions, as well as ellipticity of the calculated behavior [18–21];
  - exact equivalence between stress-based and strain-based formulations;
  - result is independent of the geometric period chosen.

In order to reach a conclusion regarding the choice of the UHT, two considerations should be adopted. First, the quality of the AHT will be assessed by comparing its results with those of the

UHT. Second, the AHT should not be influenced by intrinsic shortcomings of the UHT, so that the assessment remains unbiased.

Accordingly, to ensure the most reliable comparison framework, the PHT is preferred to the EMHT. This choice arises from the well-known limitations of the EMHT, which introduce uncertainties in direct comparisons and may obscure the assessment of whether incorporating the fractal geometric construction into the AHT is judicious.

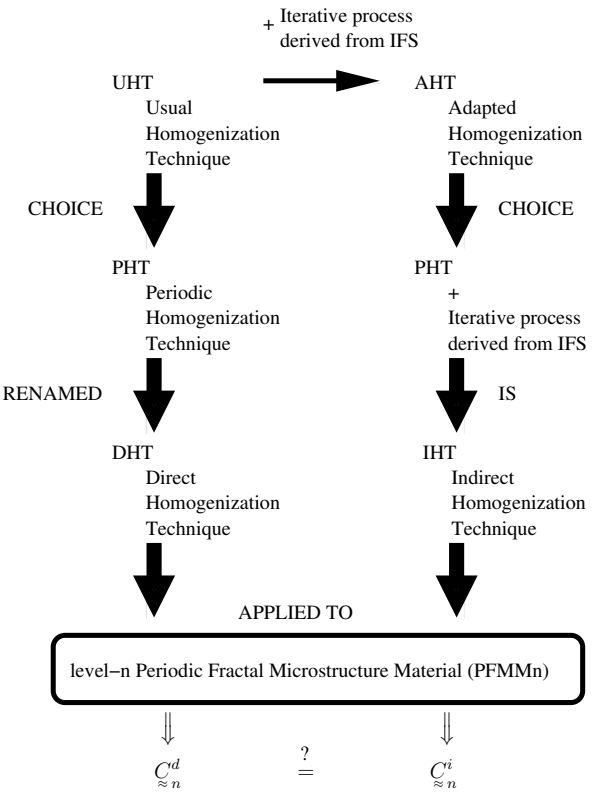

Figure 1. Schematic representation of the acronyms and their relationships.

Finally (Figure 1):

- The evaluation of the equivalent properties of an FMMn requires first identifying the UHT. Since the PHT is selected, the AHT will be defined on its basis. This choice implies that the Representative Volume Element (RVE) of the studied material is assumed to be periodic, with its geometry defined by the repetition of a fundamental pattern referred to as the periodic cell, which in the present study has a fractal geometry.
- As will be shown later, the construction of a level-n fractal geometry is based on an iterative process. The objective is to incorporate a similar process into the UHT, thereby defining the AHT.
- The UHT corresponds to the homogenization technique that evaluates the properties of the FMMn directly on its level-n fractal geometry. In the following, this approach will be referred to as the Direct Homogenization Technique (DHT). The DHT thus constitutes the reference method on which the AHT is built.
- The AHT can then be identified as the DHT enriched by the iterative process that generates the fractal geometry. For this reason, it will be called the Indirect Homogenization Technique

(IHT). The working assumption is that the IHT evaluates the properties of the FMMn by performing calculations on a lower-level fractal geometry, while maintaining equivalent accuracy to the DHT.

The main challenge of this study is to validate this hypothesis in the case of periodic FMMn (PFMMn) by comparing the equivalent fourth-order elasticity tensors $\underset{\approx}{C}_n^d$ and $\underset{\approx}{C}_n^i$, obtained respectively using the DHT and the IHT (Figure 1).

3. A quick reminder about fractals

3.1. *Scope of the present study*

The purpose of this study is not to conduct an in-depth mathematical analysis of fractal theory, which can be found in specialized works such as those of Gentil et al. [22] or Gouyet [23]. Instead, the focus is on providing a clear understanding of how fractal geometries can be constructed in a systematic and reproducible way. For this purpose, the Iterated Function Systems (IFS) concept is adopted. Beyond serving as a tool for generating controlled fractal geometries, the IFS also provides the framework that allows this construction process to be embedded into the DHT, thereby defining the IHT.

3.2. *IFS and self-similarity*

In this study, the focus was exclusively on fractal geometries based on the exact self-similarity property, as introduced by Hutchinson [24] in 1981 through the IFS formalism. Consequently, it is essential to define this construction methodology and to establish a comprehensive vocabulary.

- The physical space ε^3 is modeled as a Euclidean affine space. The reference frame is $R = (O, \vec{x}_1, \vec{x}_2, \vec{x}_3)$ where $b = (\vec{x}_1, \vec{x}_2, \vec{x}_3)$ denotes an orthonormal basis, and O represents the origin. The set of non-empty compacts of ε^3 is denoted $C(\varepsilon^3)$.
- An IFS, denoted as I, is defined as a finite set of N contractive transformations, $(T_i)_{i=0,\dots,N-1}$:

$$I = \left\{(T_i)_{i=0,\dots,N-1} \;/\; T_i : \varepsilon^3 \to \varepsilon^3\right\}, \tag{1}$$

  each transformation T_i acts on points. By extension, it can also be defined to act on objects as follows: for an object K in $C(\varepsilon^3)$, its image K' under T_i is given by $K' = T_i(K)$, if and only if:

$$K' = T_i(K) = \left\{T_i(M),\ \forall\ M \in K\right\}. \tag{2}$$

- The Hutchinson operator, denoted $\mathbb{T}$ [25], and the attractor of the IFS, denoted as A, are defined as follows:

$$\mathbb{T} = \bigcup_{i=0}^{N-1} T_i, \qquad \begin{cases} A_0 \text{ given} \\ A_n = \mathbb{T}(A_{n-1}) = \mathbb{T}^n(A_0) \\ A = \lim\limits_{n \to +\infty} \mathbb{T}(A_n) \end{cases} \tag{3}$$

  where A_0 is designated as the primitive (initial object) and A_n is referred to as the level-n geometry, which provides an approximation to the attractor A. It has been demonstrated that the Hutchinson operator is contractive with respect to the Hausdorff distance [25], and that there exists a unique object a such that $a = \mathbb{T}(a)$. This result, known as the fixed point theorem, implies that the attractor is independent of the primitive A_0. Consequently, $a = A$, and

$$\mathbb{T}(A) = A \tag{4}$$

  defines the unique attractor of the IFS.

- An object K possesses the self-similarity property with respect to an IFS if $K = \mathbb{T}(K)$. This property ensures the uniqueness of the object and identifies it as the attractor of the IFS. Consequently, the object is composed of multiple smaller copies of itself. Each copy is obtained through a transformation T_i, and each of these copies is itself composed of smaller copies, continuing ad infinitum. This property implies that the object can only be accessed through iterative processes (eq. 3) [22].

3.3. *Fractal geometries studied and convergence at infinity*

In this study, several fractal geometries based on the IFS principle were considered as the periodic cell of the PFMMn. For all the geometries studied, the set of transformations in the considered IFS consists of different affine transformations, but their linear part is the same. The initial configurations investigated were two-dimensional (2D) and extruded in the direction normal to their plane. The geometries examined (Figure 2) include the Sierpiński carpet, the Sierpiński hexagon, the filled Sierpiński hexagon (also known as hexaflake fractal), the Vicsek fractal in saltire form, and Vicsek fractal in cross form. The main motivation for selecting these geometries was to accelerate the acquisition of results across different configurations and to enable a more straightforward analysis compared with fully three-dimensional (3D) geometries. This approach provides an initial methodological framework for validating the IHT. Considering the high contrast between phases (voids and solid matter), another motivation for selecting these geometries is that the rule of mixtures appears to provide a reasonable approximation of the fourth-order elasticity tensor component representing the stiffness along the extrusion direction. It therefore offers a simple model for comparison with the IHT results. Finally, the identified concepts and techniques were extended to a 3D geometry, specifically the Menger sponge (Figure 3), in order to address higher levels of complexity. This extension also increases the size of the numerical problems to be solved and serves to further assess the relevance of the IHT.

It should be noted that the volume of the solid phase of a fractal geometry tends to zero as the iteration level-n tends to infinity. Consequently, the measure of the integration domain in the integrals used to compute the homogenized fourth-order elasticity tensor $\underset{\approx}{C}{}_n^H$ also tends to zero. Therefore, theoretically, $\lim_{n\to\infty} \underset{\approx}{C}{}_n^H = \underset{\approx}{C}_{\text{void}}$, where $\underset{\approx}{C}_{\text{void}}$ denotes the fourth-order elasticity tensor of the void if it is considered as a material. In most cases, $\underset{\approx}{C}_{\text{void}} = \underset{\approx}{0}$. However, in order to evaluate the accuracy of the IHT, two cases must be distinguished:

- 2D extruded geometries: since these lead to smaller discretizations than fully 3D cases, the void is meshed and assigned a nonzero elasticity tensor ($\underset{\approx}{C}_{\text{void}} \neq \underset{\approx}{0}$). It is modeled as an isotropic material with a Young's modulus $E_v = 185$ MPa (one-twentieth of the Young's modulus of the solid phase constituent material) and a Poisson's ratio $\nu = 0.3$. In this case, the expected convergence is $\lim_{n\to\infty} \underset{\approx}{C}{}_n^i = \underset{\approx}{C}_{\text{void}}$, and this should be observed;
- 3D geometries: the void is not meshed. Accordingly, the convergence to be observed is $\lim_{n\to\infty} \underset{\approx}{C}{}_n^i = \underset{\approx}{0}$.

4. Implementation of the IHT

4.1. *Study framework*

The framework adopted for this study may appear restrictive. However, such restriction is necessary given the exploratory nature of the work. It is also essential to focus on cases that allow a clear assessment of the approach, both in terms of its soundness and its potential for further development.

Because the number of DOFs increases rapidly with the fractal iteration level, computing the effective mechanical behavior of a PFMMn with the DHT quickly becomes impractical. By contrast, the IHT can be applied to much higher iteration levels, and even considered in the limit as $n \to \infty$. Therefore, direct validation of the IHT against the DHT is only possible for the first iteration levels, which remain computationally accessible.

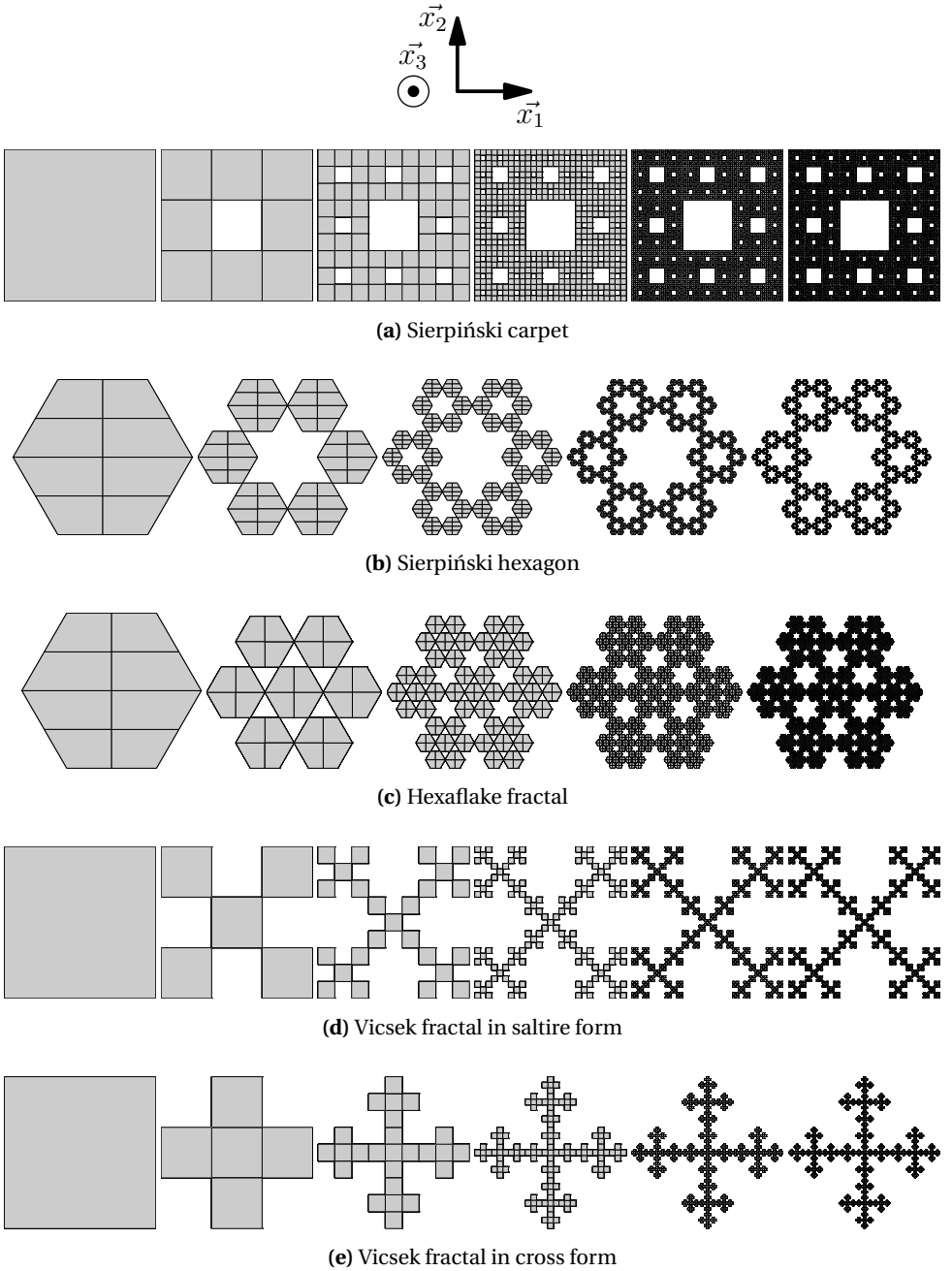

(a) Sierpiński carpet

(b) Sierpiński hexagon

(c) Hexaflake fractal

(d) Vicsek fractal in saltire form

(e) Vicsek fractal in cross form

Figure 2. Five extruded 2D fractal geometries at different iteration levels.

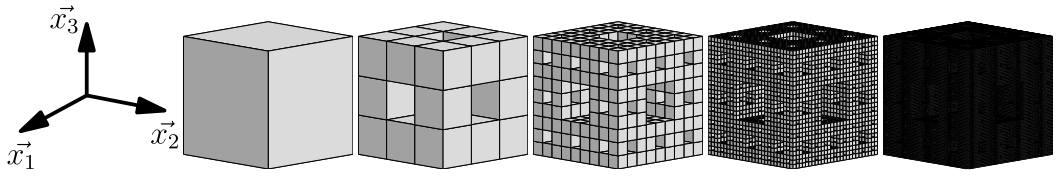

Figure 3. Menger sponge at iteration levels 0 to 4.

4.2. *Exploration of IHT and DHT techniques: functionality and distinctions*

As mentioned previously, the objective of this study is to evaluate the equivalent mechanical behavior of PFMMn, in particular the homogenized fourth-order elasticity tensor, denoted $\underset{\approx}{C}^H_n$. This section presents the operating principles of the IHT and DHT, and highlights the methodological differences between them.

The IHT begins by homogenizing the level-1 geometry, denoted A_1, using the constituent material behavior $\underset{\approx}{C}_0$. This constituent is assumed to be isotropic, characterized by a Young's modulus of $E = 3700$ MPa and a Poisson's ratio of $\nu = 0.3$ (values typical of polymers, i.e., potential candidates for fabricating such microstructures). The resulting homogenized elasticity tensor is denoted $\underset{\approx}{C}^i_1$, where the superscript i refers to the "indirect" nature of the IHT. In the next step, the same geometry A_1 is re-homogenized, but using the effective behavior $\underset{\approx}{C}^i_1$. Repeating this process iteratively yields the effective behavior at level-n, denoted $\underset{\approx}{C}^i_n$. This is obtained by successively homogenizing the same geometry A_1, while updating at each iteration the constitutive behavior of its solid phase with the effective behavior obtained at the previous one. In other words, $\underset{\approx}{C}^i_2$ is obtained by assigning $\underset{\approx}{C}^i_1$ as the constitutive behavior of A_1, $\underset{\approx}{C}^i_3$ by assigning $\underset{\approx}{C}^i_2$, and so on, until $\underset{\approx}{C}^i_n$ is obtained from $\underset{\approx}{C}^i_{n-1}$. Thus, the geometry remains fixed, while the constitutive behavior of its solid phase is progressively updated with the effective properties from the previous iteration.

By contrast, the DHT proceeds by iterating on the geometry itself. Once the fractal geometry A_n at iteration level-n is constructed, direct homogenization is performed on A_n using the initial constituent behavior $\underset{\approx}{C}_0$. The resulting effective behavior is denoted $\underset{\approx}{C}^d_n$, where the superscript d indicates the "direct" nature of the DHT.

A comparison between $\underset{\approx}{C}^i_n$ and $\underset{\approx}{C}^d_n$ thus provides a measure of the IHT's accuracy, in addition to the convergence at infinity (see Section 3.3). As illustrated in Figure 4, the Menger sponge is used to show the algorithmic flowcharts of both techniques, thereby clarifying the distinctions between them.

4.3. *Calculation methodology*

The next step involves the execution of homogenization calculations employing both DHT and IHT techniques. Calculations and meshes were performed using the Z-set software [26].

A mesh convergence study was performed on the level-1 cell, A_1, in order to select a reliable reference mesh. The convergence criterion was based on the homogenized elasticity tensor: refinement was continued until the variation of its components fell below 1%. Quantitatively, the relative error between two successive refinements was computed as follows:

$$e_r = \left| \frac{c^d_{jk,n,r_i} - c^d_{jk,n,r_{i+1}}}{c^d_{jk,n,r_{i+1}}} \right| \times 100 \tag{5}$$

where c^d_{jk,n,r_i} are the homogenized elasticity tensor components, in the usual Voigt notation, of cell A_n with r_i mesh refinement, obtained by the DHT.

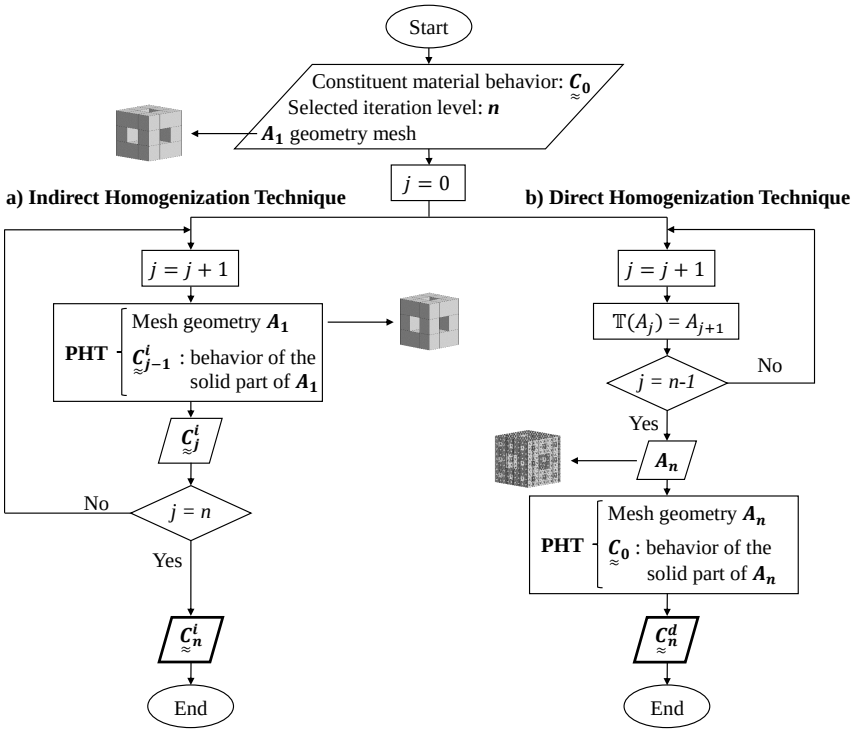

Figure 4. Algorithmic flowcharts for the IHT and DHT techniques.

Once this reference mesh was validated, it was first used to carry out the IHT. The same mesh was then used as the basis for generating higher-level meshes: the IFS was applied to the mesh of A_1 to construct the meshes of $A_2, A_3, \ldots, A_n$, which were subsequently employed in the DHT. This procedure guarantees mesh consistency across all iteration levels and eliminates any bias from finite element discretization when comparing the effective properties obtained with the DHT and those obtained with the IHT.

In practice, the generation of meshes could only be achieved up to a certain fractal iteration level, with the limitation being more restrictive in 3D than in 2D due to the rapid growth in complexity.

5. Results and discussion

5.1. *Volume and density of matter of the level-*$(n+1)$ *geometry*

Since the homogenization process relies on the concept of averaging over the entire cell (volume V_{cell}, including both void and solid matter), it has been verified that the volume of matter V_m^{n+1} in the level-$(n+1)$ geometry obtained through the iterative process is exactly equal to the theoretical value, assuming $V_m^0 = V_{\text{cell}}$. This result confirms that no error is introduced by the averaging operation in the IHT process. Accordingly, the matter density $\rho_m^{n+1} = V_m^{n+1}/V_{\text{cell}}$ and the void density $\rho_v^{n+1} = 1 - \rho_m^{n+1}$ are correctly evaluated. It is important to note, however, that if the level-0 geometry already contains voids (*primary voids*, as opposed to the *conformation voids* induced by the IFS), i.e. $V_m^0 \neq V_{\text{cell}}$, the iterative process leads to an incorrect evaluation of V_m^{n+1} and ρ_m^{n+1}, and consequently to an incorrect evaluation of the homogenized tensor $\underset{\approx}{C}^i_{n+1}$.

5.2. *Extruded 2D fractal geometries*

This section presents the homogenization results for extruded 2D fractal geometries. For detailed analysis, the extruded Sierpiński carpet is chosen as a representative geometry.

Table 1 compares the components of the homogenized elasticity tensor for iteration levels 1 to 6, with level 0 (the constituent material) provided as a common reference. Since this is an extruded 2D geometry, only the in-plane tensor components and the normal stiffness component along the extrusion direction (c_{33}) are considered. The latter is also compared with the rule of mixtures estimate. The homogenized elasticity tensor belongs to the cubic symmetry class. For levels 5 and 6, asterisks denote DHT values obtained from meshes that were not derived from the same converged level-1 reference mesh as in lower levels, and may therefore include discretization bias.

Table 1. Homogenized elasticity tensor components of the extruded Sierpiński carpet cell for iteration levels 0 to 6, obtained by DHT, IHT, and the rule of mixtures identified by the superscripts d, i, and m respectively. Asterisks denote DHT values obtained from meshes that were not derived from the same converged level-1 reference mesh as in lower levels. ρ_m^n and ρ_v^n denote, respectively, the matter and void densities at level n.

Constituent material (level-0) ($\boldsymbol{\rho_m^0 = 1.00}$, $\boldsymbol{\rho_v^0 = 0.00}$)								
$c_{11}^0 = c_{22}^0 = c_{33}^0$ (MPa)			c_{12}^0 (MPa)			c_{66}^0 (MPa)		
4981			2135			1423		
Iteration level-1 ($\boldsymbol{\rho_m^1 = 0.89}$, $\boldsymbol{\rho_v^1 = 0.11}$)								
c_{11}^d	c_{11}^i	c_{12}^d	c_{12}^i	c_{66}^d	c_{66}^i	c_{33}^d	c_{33}^i	c_{33}^m
3661	3661	1375	1375	969	969	4216	4216	4460
Iteration level-2 ($\boldsymbol{\rho_m^2 = 0.79}$, $\boldsymbol{\rho_v^2 = 0.21}$)								
c_{11}^d	c_{11}^i	c_{12}^d	c_{12}^i	c_{66}^d	c_{66}^i	c_{33}^d	c_{33}^i	c_{33}^m
2801	2765	947	932	677	687	3637	3628	3987
Iteration level-3 ($\boldsymbol{\rho_m^3 = 0.70}$, $\boldsymbol{\rho_v^3 = 0.30}$)								
c_{11}^d	c_{11}^i	c_{12}^d	c_{12}^i	c_{66}^d	c_{66}^i	c_{33}^d	c_{33}^i	c_{33}^m
2193	2137	683	665	498	507	3171	3158	3561
Iteration level-4 ($\boldsymbol{\rho_m^4 = 0.62}$, $\boldsymbol{\rho_v^4 = 0.38}$)								
c_{11}^d	c_{11}^i	c_{12}^d	c_{12}^i	c_{66}^d	c_{66}^i	c_{33}^d	c_{33}^i	c_{33}^m
1753	1689	516	499	383	389	2788	2773	3182
Iteration level-5 ($\boldsymbol{\rho_m^5 = 0.55}$, $\boldsymbol{\rho_v^5 = 0.45}$)								
$c_{11}^{d^*}$	c_{11}^i	$c_{12}^{d^*}$	c_{12}^i	$c_{66}^{d^*}$	c_{66}^i	$c_{33}^{d^*}$	c_{33}^i	c_{33}^m
1432	1363	409	391	308	309	2467	2451	2851
Iteration level-6 ($\boldsymbol{\rho_m^6 = 0.49}$, $\boldsymbol{\rho_v^6 = 0.51}$)								
$c_{11}^{d^*}$	c_{11}^i	$c_{12}^{d^*}$	c_{12}^i	$c_{66}^{d^*}$	c_{66}^i	$c_{33}^{d^*}$	c_{33}^i	c_{33}^m
1208	1123	340	320	260	254	2198	2179	2567

Two complementary analyses are considered to compare the results of IHT and DHT, while also highlighting the advantages and capabilities of the IHT.

The first (Figure 5) illustrates the evolution of the homogenized elasticity tensor components obtained with both techniques across iteration levels. Normalization is carried out with respect to the homogeneous level-0 cell components, which are those of the constituent material. The plotted values confirm the overall consistency of the two methods, with only minor discrepancies. They also emphasize a practical advantage of the IHT: the method remains applicable at high iteration levels, whereas the DHT becomes increasingly limited beyond level 6.

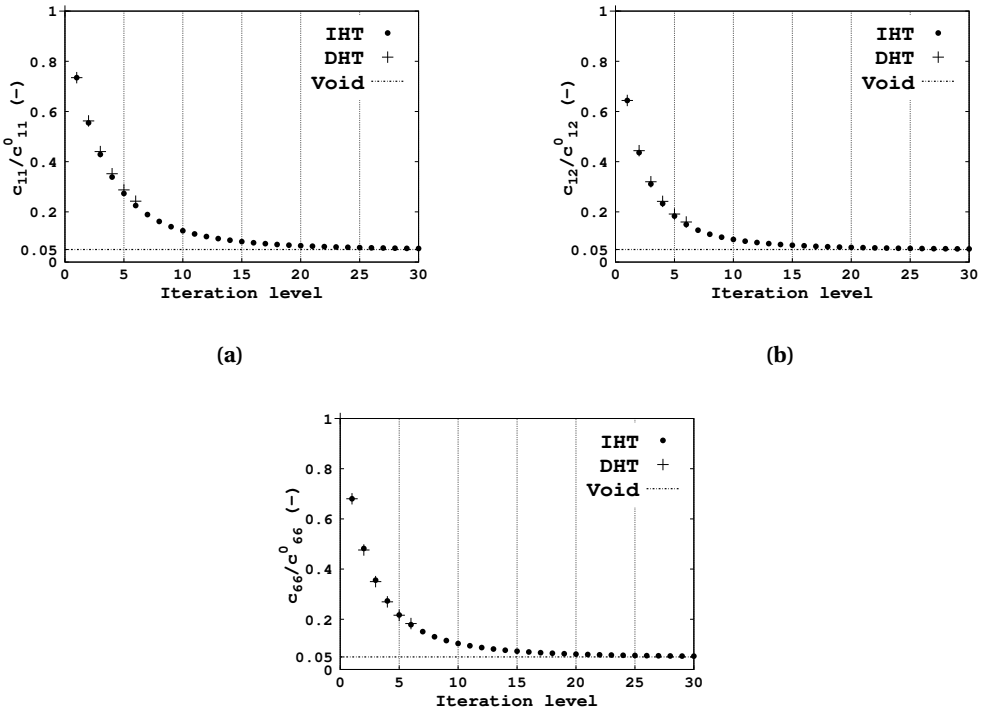

Figure 5. Sierpiński carpet. Comparative analysis of the normalized components of the homogenized elasticity tensor: (a) c_{11}/c^0_{11}, (b) c_{12}/c^0_{12}, and (c) c_{66}/c^0_{66}. The IHT (dots) vs. DHT (crosses) at different iteration levels. The results of the IHT converge towards the components of the elasticity tensor of the meshed void.

Table 2. Quantitative analysis of the relative difference, measured in percentages, between the IHT and DHT results of the homogenized elasticity tensor components for the initial 6 iteration levels. The considered periodic cell is the Sierpiński carpet. In addition, a comparison of computational time requirements and DOFs between these techniques.

	Error (%)			**DHT**		**IHT**	
Iteration level	c_{11}	c_{12}	c_{66}	Computing time	DOFs	Computing time	DOFs
1	0	0	0	few seconds	≈ 50 000	few seconds	≈ 50 000
2	1.3	1.6	1.5	≈ 20 minutes	≈ 650 000	few seconds	≈ 50 000
3	2.6	2.6	1.8	≈ 3 hours	≈ 2 600 000	few seconds	≈ 50 000
4	3.7	3.3	1.6	≈ 6 hours	≈ 6 000 000	few seconds	≈ 50 000
5*	4.8	4.4	0.3	≈ 1/2 day	≈ 13 300 000	few seconds	≈ 50 000
6*	7	5.9	2.3	> 1/2 day	≈ 20 000 000	few seconds	≈ 50 000

A clear asymptotic trend emerges from the IHT results. As the fractal iteration level increases, each homogenized elasticity tensor component decreases monotonically toward the value of the meshed void phase (dashed lines in the plots). This behavior is physically expected because the solid volume fraction decreases monotonically with each iteration, while the void fraction

increases, leading the effective response to be dominated by the void phase. Extending the IHT to about 30 iterations clearly illustrates this asymptotic convergence. In this respect, the IHT reproduces the DHT at moderate levels and, moreover, makes it possible to reach higher iteration levels from which the asymptotic behavior can be reliably inferred, a regime that remains inaccessible to DHT in practice.

The second comparison quantifies the relative error (Table 2) for each elasticity tensor component, defined as: $e = \left| \frac{c^d_{jk} - c^i_{jk}}{c^d_{jk}} \right| \times 100$. For iteration levels 1 to 4, the errors remain small, with a maximum of 3.7%. At levels 5 and 6, the discrepancies are slightly larger, up to 7%, which is explained by the fact that the corresponding DHT meshes could not be generated from the same converged level-1 reference mesh. Overall, the agreement between the two techniques is very good, confirming that IHT reproduces DHT within a narrow tolerance across all accessible levels.

Finally, the relative error between the c_{33} component obtained with the IHT (c^i_{33}) and the estimate given by the rule of mixtures (c^m_{33}) was evaluated as: $\left| \frac{c^m_{33} - c^i_{33}}{c^m_{33}} \right| \times 100$. The maximum error is about 10%. This additional result reinforces the reliability of the IHT as a method for evaluating the homogenized elasticity tensor of such materials.

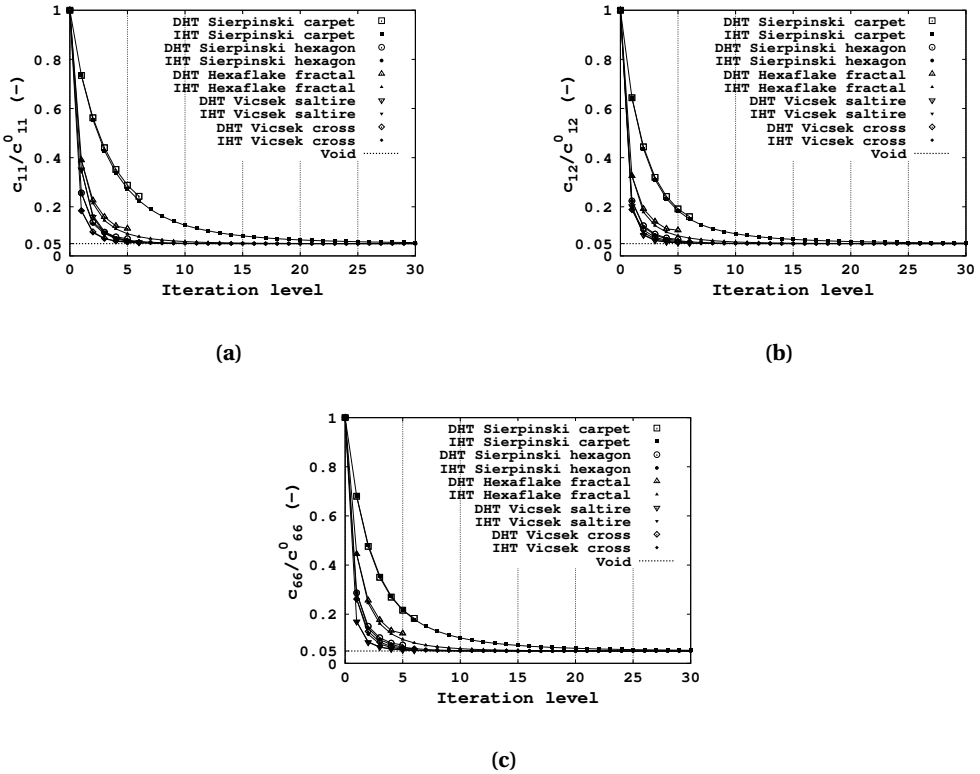

Figure 6. Comparative analysis of the normalized components of the homogenized elasticity tensor: (a) c_{11}/c^0_{11}, (b) c_{12}/c^0_{12}, and (c) c_{66}/c^0_{66}, derived from the two techniques, IHT and DHT, for each extruded 2D fractal geometry periodic cell, across various iteration levels. The results of the IHT converge towards the components of the elasticity tensor of the meshed void.

The results for all extruded 2D fractal geometries (Figure 6) are reported, with all components normalized by those of the homogeneous level-0 cell. DHT computations were performed up to level 5 for the Sierpiński hexagon and the hexaflake, and up to level 6 for the other geometries. As in the case of the Sierpiński carpet, at the first iteration levels, the IHT results coincide with those of the DHT, confirming its accuracy where direct comparisons are feasible. Unlike the DHT, however, the IHT can be extended to higher iteration levels, where it consistently converges toward the void phase properties. This systematic convergence justifies extrapolating the results to large iteration levels, and supports the interpretation that the IHT is exact in the limit $n \to \infty$.

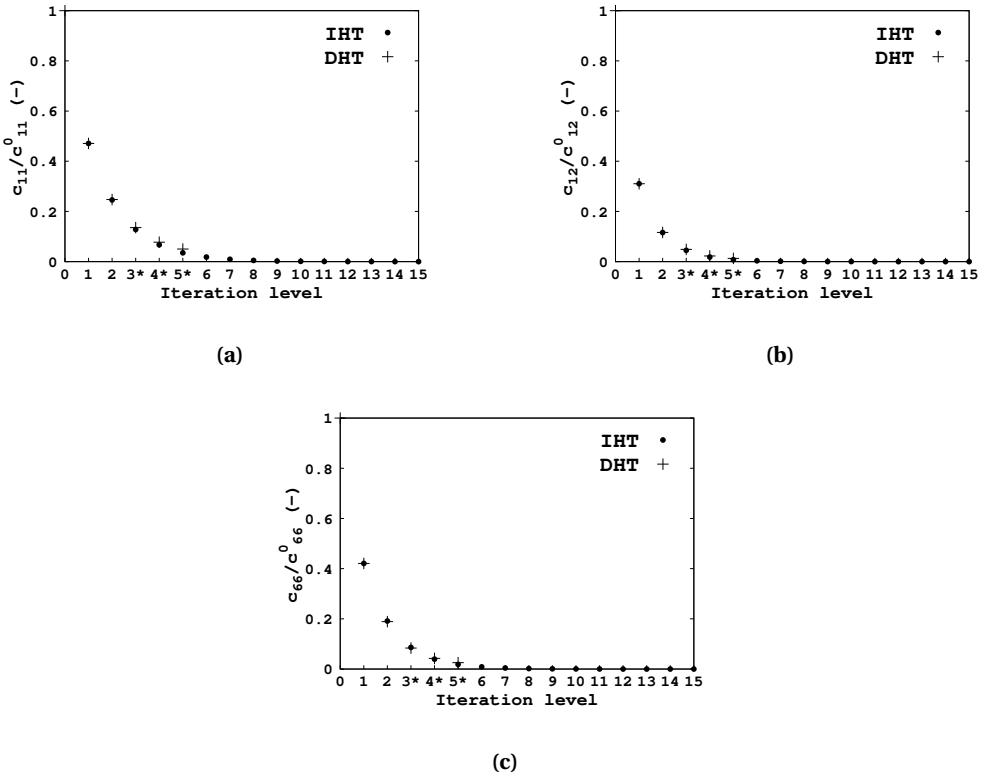

Figure 7. Menger sponge. Comparative analysis of the normalized components of the homogenized elasticity tensor: (a) c_{11}/c^0_{11}, (b) c_{12}/c^0_{12}, and (c) c_{66}/c^0_{66}. The IHT (dots) vs. DHT (crosses) at different iteration levels. In the absence of void meshing, the results of the IHT converge towards zero values. The resulting homogenized material is cubic, so: $c_{11} = c_{22} = c_{33}$, $c_{12} = c_{13} = c_{23}$, and $c_{44} = c_{55} = c_{66}$. Asterisks denote DHT values obtained from meshes that were not derived from the same converged level-1 reference mesh as in lower levels.

5.3. *3D fractal geometry: Menger sponge*

Homogenization calculations using both techniques were carried out for the 3D case of the Menger sponge cell. All components of the homogenized elasticity tensor are normalized by those of the homogeneous level-0 cell (Figure 7). The tensor exhibits cubic symmetry. As in the

extruded 2D cases, the two techniques show close agreement at the first iteration levels where direct comparisons are possible, thereby confirming the accuracy of the IHT.

A key difference from the 2D analyses is that, in 3D, the void is not meshed. Consequently, as the iteration level increases, the components of the homogenized elasticity tensor decrease monotonically and converge toward zero, i.e., $\underset{\approx}{C}{}_n^H \to \underset{\approx}{0}$ as $n \to \infty$. This convergence can only be revealed by the IHT, which enables computations beyond the range accessible by the DHT. Hence, the IHT not only reproduces the expected trend but also justifies extrapolating it to arbitrarily large iteration levels, and supports the interpretation that, in the 3D case as well, the IHT is exact in the limit $n \to \infty$.

5.4. *DHT versus IHT*

Beyond the consistency of the effective properties, an important distinction between the two homogenization strategies lies in their numerical requirements. The IHT relies on a single converged mesh defined at the level-1 cell, which is reused at all iteration levels. In contrast, the DHT requires explicit homogenization on each fractal geometry, with meshes that grow rapidly in size as the iteration level increases.

The comparison reported in Table 2 highlights the strong numerical efficiency of the IHT. Computation times remain nearly constant across iteration levels, since only the material behavior assigned to the level-1 cell is updated from one iteration to the next. By contrast, the DHT exhibits a steep increase in cost, both in memory and time, which restricts its applicability to relatively low fractal levels.

This cost-effectiveness is a key advantage of the IHT, since it makes the study of a PFMMn feasible at iteration levels that remain inaccessible to the DHT.

5.5. *Remarks on the periodicity conditions of level-n embedded in level-*$(n+1)$

The level-$(n+1)$ cell is considered periodic, i.e., it is embedded within a periodic environment for which it defines the representative period. However, the level-n geometry within the level-$(n+1)$ cell is no longer in the same periodic environment as that used for the evaluation of its own properties. This raises an important question: why do the periodic properties of the level-n geometry, when used in the periodic homogenization of the level-$(n+1)$ cell, still yield good results? At present, there is no definitive answer to this question, but two plausible explanations can be proposed:

- The periodicity conditions of the level-n geometry within the level-$(n+1)$ cell are quasi-verified, as is the case for Menger sponges. The concept of quasi-periodicity in fractal geometries [27,28], if it can be demonstrated, would support this explanation.
- The periodicity conditions have only a limited influence on the homogenized properties. This is particularly true for the extruded 2D geometries considered here: the surface area of the level-$(n+1)$ periodic cell affected by the periodic boundary conditions may represent only a small fraction of its total surface, and the geometric connections between level-n geometries within the level-$(n+1)$ cell are very limited and essentially non-surfacic.

5.6. *On non-linear behavior and large-strain theory*

At present, the IHT process only considers matter with linear elastic behavior under the assumption of small perturbations. This represents the most favorable framework to avoid uncertainties

related to the periodic homogenization process. But what happens outside this framework? If a non-linear behavior such as linear viscoelasticity is considered for the solid phase, the Laplace transformation leads, in the Laplace space, to equations that are similar to those of the linear elastic case. Without returning to the real space, it can therefore be stated that if the IHT is well suited and accurate for the linear elastic case under the small-perturbation hypothesis, it should also be well suited and accurate for the linear viscoelastic case under the same assumption. For other types of non-linear material behavior, the homogenization process generally captures the response curve point by point rather than providing an identified effective property from a single computation. It is therefore not clear what advantage the IHT would offer in such cases, or even whether it would remain applicable. In any case, the IHT method should be used with caution when the model is likely to induce local volume variations or significant local geometric changes not included in the IFS construction (see Section 5.1). The assumption of small perturbations naturally avoids such difficulties.

5.7. *From a practical point of view*

From a practical point of view, once a given weight reduction and an acceptable target property are defined for a structure, the IHT process makes it possible to explore a wide range of microstructural geometries. For each geometry, both the weight gain and the corresponding loss in mechanical property can be evaluated (Figure 8), allowing the most suitable configuration to be selected. However, an important point should be noted: although the fraction of matter (or void) in a fractal geometry can usually be evaluated analytically, the evolution of this fraction and that of the corresponding effective property do not follow the same trend (Figure 8). The use of the IHT process is therefore essential for an accurate assessment of the effective material properties.

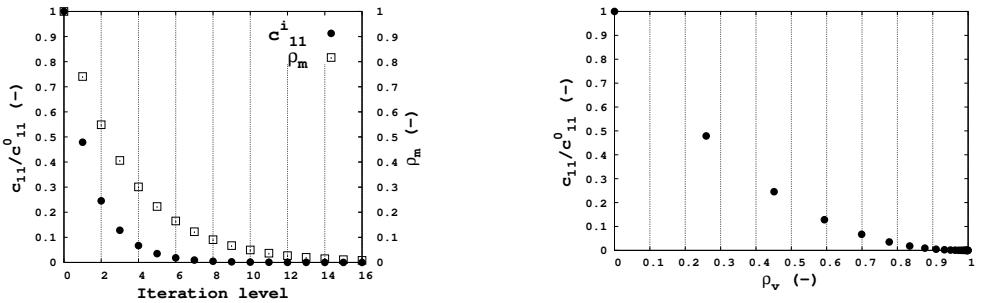

(a) **(b)**

Figure 8. (a) Evolution of the matter volume fraction ρ_m and of a normalized component of the homogenized elasticity tensor, c_{11}/c^0_{11}, with respect to the iteration level. (b) Evolution of c_{11}/c^0_{11} as a function of the void volume fraction, $\rho_v = 1 - \rho_m$.

6. Conclusion

This study addressed the homogenization of PFMMn. The intrinsic complexity of their geometries makes the use of conventional homogenization methods problematic, since the number of DOFs grows rapidly with the iteration level, leading to numerical models of considerable size.

To overcome this limitation, the IHT was developed on the basis of the DHT, by embedding the iterative process that generates the fractal geometry into the homogenization procedure. Both techniques were applied to 2D extruded geometries and to a 3D case. The comparison showed that, for iteration levels where both techniques could be applied, the results of IHT and DHT were in very close agreement. In addition, the IHT requires significantly lower computational cost, in terms of both computation time and memory, and therefore remains applicable at iteration levels that cannot be reached by the DHT.

Beyond this direct validation, the IHT also demonstrated an essential property: at higher iteration levels, where the DHT could not be applied, the homogenized elasticity tensor obtained by the IHT converges toward that of the void. This behavior is physically consistent with the progressive reduction of solid volume fraction and provides an indirect but convincing verification of the accuracy of the IHT at iteration levels inaccessible to the DHT.

The scope of this work was intentionally restricted to exact self-similarity and periodic geometries, with the objective of establishing a solid methodological basis. The results obtained confirm both the accuracy and the efficiency of the IHT and provide a reliable foundation for future extensions toward more complex cases, including approximate self-similarity and non-linear behavior.

Acknowledgments

The manuscript was written through contributions of all authors.

Declaration of interests

The authors do not work for, advise, own shares in, or receive funds from any organization that could benefit from this article, and have declared no affiliations other than their research organizations.

References

[1] B. Mandelbrot, *Fractals: form, chance and dimension*, Freeman, 1977.

[2] D. Pence, "The simplicity of fractal-like flow networks for effective heat and mass transport", *Exp. Therm. Fluid Sci.* **34** (2010), no. 4, pp. 474–486.

[3] I. M. Rian and M. Sassone, "Tree-inspired dendriforms and fractal-like branching structures in architecture: a brief historical overview", *Front. Archit. Res.* **3** (2014), no. 3, pp. 298–323.

[4] C. Puente, J. Romeu, R. Pous, X. Garcia and F. Benitez, "Fractal multiband antenna based on the Sierpinski gasket", *Electron. Lett.* **32** (1996), no. 1, pp. 1–2.

[5] N. Cohen, "Fractal antenna applications in wireless telecommunications", in *Professional Program Proceedings. Electronic Industries Forum of New England*, IEEE, 1997, pp. 43–49.

[6] S. C. Soo, K. M. Yu and W. K. Chiu, "Modeling and fabrication of artistic products based on IFS fractal representation", *Comput.-Aided Des.* **38** (2006), no. 7, pp. 755–769.

[7] V. Linares, A. Aguilar-de-Leyva, M. Casas and I. Caraballo, "3D printed fractal-like structures with high percentage of drug for zero-order colonic release", *Pharmaceutics* **14** (2022), no. 11, article no. 2298.

[8] V. Nguyen-Van, C. Wu, F. Vogel, G. Zhang, H. Nguyen-Xuan and P. Tran, "Mechanical performance of fractal-like cementitious lightweight cellular structures: numerical investigations", *Compos. Struct* **269** (2021), article no. 114050.

[9] M. Viccica, M. Galati, F. Calignano and L. Iuliano, "An additively manufactured fractal structure for impact absorption applications", *Procedia CIRP* **118** (2023), pp. 793–798.

[10] P. Pavón-Domínguez, G. Portillo-García, A. Rincón-Casado and L. Rodríguez-Parada, "Influence of the fractal geometry on the mechanical resistance of cantilever beams designed through topology optimization", *Appl. Sci. (Switz.)* **11** (2021), no. 22, article no. 10554 (13 pages).

[11] M. Viccica, M. Galati, F. Calignano and L. Iuliano, "Design, additive manufacturing, and characterisation of a three-dimensional cross-based fractal structure for shock absorption", *Thin-Walled Struct.* **181** (2022), article no. 110106.
[12] M. Zhao, H. Qing, Y. Wang, J. Liang, M. Zhao, Y. Geng, J. Liang and B. Lu, "Superelastic behaviors of additively manufactured porous NiTi shape memory alloys designed with Menger sponge-like fractal structures", *Mater. Des.* **200** (2021), article no. 109448 (12 pages).
[13] A. S. Ullah, D. M. D'Addona, Y. Seto, S. Yonehara and A. Kubo, "Utilizing fractals for modeling and 3D printing of porous structures", *Fractal and Fractional* **5** (2021), no. 2, article no. 40 (19 pages).
[14] D. Mohotti, D. Weerasinghe, M. Bogahawaththa, H. Wang, K. Wijesooriya and P. J. Hazell, "Quasi-static and dynamic compressive behaviour of additively manufactured Menger fractal cube structures", *Def. Technol.* **37** (2024), pp. 39–49.
[15] B. Budiansky, "On the elastic moduli of some heterogeneous materials", *J. Mech. Phys. Solids* **3** (1965), no. 4, pp. 223–227.
[16] A. Bensoussan, J. L. Lions and G. Papanicolaou, *Asymptotic analysis for periodic structure*, North-Holland, 1978.
[17] M. Berveiller and A. Zaoui, "Méthodes self-consistantes en mécanique des solides hétérogènes", in *Comportements rhéologiques et stucture des matériaux* (C. Huet and A. Zaoui, eds.), Cahiers du Groupe français de rhéologie, vol. 15, ENPC, 1981, pp. 175–199.
[18] P. Suquet, *Plasticité et homogénéisation*, PhD thesis, Université Paris VI (France), 1982.
[19] F. Léné, *Contribution à l'étude des matériaux composites et de leur endommagement*, PhD thesis, Université Paris VI (France), 1984.
[20] H. Dumontet, *Homogénéisation et effets de bords dans les matériaux composites*, PhD thesis, Université Paris VI (France), 1990.
[21] J. Sanchez-Hubert and E. Sanchez-Palencia, *Introduction aux méthodes asymptotiques et à l'homogénéisation*, Masson, 1992.
[22] C. Gentil, G. Gouaty and D. Sokolov, *Geometric modeling of fractal forms for CAD*, John Wiley & Sons, 2021.
[23] J. F. Gouyet, *Physique et structures fractales*, Masson, 1992.
[24] J. E. Hutchinson, "Fractals and self similarity", *Indiana Univ. Math. J.* **30** (1981), no. 5, pp. 713–747.
[25] M. Barnsley, *Fractals everywhere*, Academic Press Inc., 1988.
[26] ARMINES, ONERA and TRANSVALOR S.A., *Z-set*, version 9.1.6, 2020. Online at http://www.zset-software.com (accessed on November 13, 2025).
[27] E. Esclangon, "Les fonctions quasi-périodiques", in *Thèses présentées à la faculté des sciences de Paris pour obtenir le grade de docteur ès sciences mathématiques*, Thèses de la faculté des sciences de Paris, vol. 1187, Gauthier-Villars, 1904, pp. 1–276.
[28] J. Favard, *Leçons sur les fonctions presque-périodiques*, Gauthier-Villars, 1933.